

# Simultaneous calcium fluorescence imaging and MR of *ex vivo* organotypic cortical cultures: a new test bed for functional MRI<sup>†</sup>

Ruiliang Bai<sup>a,b</sup>, Andreas Klaus<sup>c</sup>, Tim Bellay<sup>c</sup>, Craig Stewart<sup>c</sup>, Sinisa Pajevic<sup>d</sup>, Uri Nevo<sup>e</sup>, Hellmut Merkle<sup>f</sup>, Dietmar Plenz<sup>c</sup> and Peter J. Basser<sup>a\*</sup>

Recently, several new functional (f)MRI contrast mechanisms including diffusion, phase imaging, proton density, etc. have been proposed to measure neuronal activity more directly and accurately than blood-oxygen-level dependent (BOLD) fMRI. However, these approaches have proved difficult to reproduce, mainly because of the dearth of reliable and robust test systems to vet and validate them. Here we describe the development and testing of such a test bed for non-BOLD fMRI. Organotypic cortical cultures were used as a stable and reproducible biological model of neuronal activity that shows spontaneous activity similar to that of *in vivo* brain cortex without any hemodynamic confounds. An open-access, single-sided magnetic resonance (MR) "profiler" consisting of four permanent magnets with magnetic field of 0.32 T was used in this study to perform MR acquisition. A fluorescence microscope with long working distance objective was mounted on the top of a custom-designed chamber that keeps the organotypic culture vital, and the MR system was mounted on the bottom of the chamber to achieve real-time simultaneous calcium fluorescence optical imaging and MR acquisition on the same specimen. In this study, the reliability and performance of the proposed test bed were demonstrated by a conventional CPMG MR sequence acquired simultaneously with calcium imaging, which is a well-characterized measurement of neuronal activity. This experimental design will make it possible to correlate directly the other candidate functional MR signals to the optical indicia of neuronal activity in the future. Copyright © 2015 John Wiley & Sons, Ltd.

**Keywords:** MRI; functional MRI; calcium; fluorescence; BOLD; organotypic culture; brain; neuronal activity

## INTRODUCTION

Detection of neuronal activity noninvasively and *in vivo* is a *desideratum* in medicine and the neurosciences. As an example, the BRAIN Initiative (<http://braininitiative.nih.gov/>) was launched with the goal of advancing neuroimaging techniques that enable the measurement of brain function at multiple spatial and temporal scales. Owing to the many forms of MRI contrast and MRI's exquisite sensitivity to water dynamics in soft tissue,

functional MRI (fMRI) remains a promising method for the assessment of neuronal activity. The most commonly used contrast mechanism in fMRI is based on the blood-oxygenation-level dependent (BOLD) effect, which detects local hemodynamic changes, a secondary effect of neuronal activity (1–3). This indirect relationship between the BOLD fMRI signal and local neuronal activity confounds its interpretation and limits both its temporal and spatial resolution (4–6).

More recently, several non-BOLD fMRI mechanisms have been proposed to detect neuronal activity directly. These methods include, but are not limited to: (i) functional diffusion MRI to detect

\* Correspondence to: Dr P. J. Basser; 13 South Drive, Building 13, Room 3W16, Bethesda, MD 20892–5772, USA  
E-mail: [pjbasser@helix.nih.gov](mailto:pjbasser@helix.nih.gov)

a R. Bai, P. J. Basser  
Section on Tissue Biophysics and Biomimetics, PPITS, NICHD, National Institutes of Health, Bethesda, Maryland, USA

b R. Bai  
Biophysics Program, Institute for Physical Science and Technology, University of Maryland, College Park, USA

c A. Klaus, T. Bellay, C. Stewart, D. Plenz  
Section on Critical Brain Dynamics, LSN, NIMH, National Institutes of Health, Bethesda, Maryland, USA

d S. Pajevic  
Mathematical and Statistical Computing Laboratory, Division of Computational Bioscience, Center for Information Technology, NIH, Bethesda, Maryland, USA

e U. Nevo  
Department of Biomedical Engineering, Tel-Aviv University, Tel-Aviv, Israel

f H. Merkle  
Laboratory for Functional and Molecular Imaging, NINDS, National Institutes of Health, Bethesda, Maryland, USA

<sup>†</sup> This article has been contributed to by US Government employees and their work is in the public domain in the USA.

**Abbreviations used:** 1D, 1-dimensional; ACSF, artificial cerebrospinal fluid; BOLD, blood-oxygen-level dependent; CPMG, Carr–Purcell–Meiboom–Gill; D, self-diffusion coefficient; F, fluorescence signal intensity; fMRI, functional MRI; FOV, field of view; GFP, green fluorescent protein;  $I_0$ , initial signal intensity; NA, numerical aperture; OGB, Oregon Green 488 BAPTA-1; PBS, phosphate buffered saline; ppm, parts per million; Q, quality factor; R, decay rate; ROI, region of interest; SE, spin echo; SNR, signal-to-noise ratio;  $T_2$ , transverse relaxation time;  $T_{2\text{eff}}$ , effective transverse relaxation time;  $\varphi$ , phase of MR signal.

water displacements (7–10), (ii) phase MRI of changes in a local magnetic field caused by neuronal currents (11–13), (iii) Lorentz-force-effect MRI of neuronal currents (14,15), (iv) proton-density-weighted MRI (16,17), and (v) spin-lock MR methods (18,19). Although proponents of these methods have reported positive findings, most of these approaches are either still in development or have not been reproduced by a larger cohort of researchers. One obstacle to advancing this important research, e.g., convincingly demonstrating one or more of these proposed mechanisms, is the dearth of “ground truth” experiments — specifically, a means to generate reproducible neuronal activity while providing a robust and reliable MR means to detect it.

At a minimum, such an fMRI test bed should include (i) a well-characterized biological model of neuronal activity free of hemodynamic and related confounds and (ii) an independent well-established neurophysiological method to detect neuronal activity directly and simultaneously with fMR/fMRI. The *in vitro* perfused brain slice is a good choice for achieving the first goal as it has been widely used in the neuroscience community as a biological model to study neural functions since the 1950s (20–22) and has no hemodynamic artifacts. Indeed, perfused brain slices have already been used in successful MR spectroscopy and imaging experiments designed to study metabolism, neurotransmitters, ions, tissue microstructure, tissue injury, and even neuronal excitation (9,23–33).

To meet the second requirement, one of the standard neurophysiological methods — which include intracellular and extracellular electro recording, intracellular calcium imaging, membrane voltage imaging, etc. (34,35) — should be used to measure neuronal activity inside the NMR/MRI system during MR acquisition. Although the closed design and potential electromagnetic interface in MR systems make it difficult to perform these recordings together with MR acquisition, a few hybrid setups have been reported in which BOLD fMRI was recorded together with electrodes (36,37) or optical fibers (6). In other fields, one group did perform successful experiments to study single cell or cell cultures with a very technically challenging setup involving a combination of confocal and magnetic resonance microscopy (38–41). However, to our knowledge, a direct (non-BOLD) fMRI experiment that satisfies the two requirements discussed above has not yet been reported.

Here we propose and demonstrate the use of such a test bed in which MR experiments and calcium fluorescence imaging are performed simultaneously on organotypic cortical cultures from a rat. In this system, a single-sided MR system with permanent magnets was used (42). Such systems, developed in the last two decades, are portable and have been used primarily to study the proton density, relaxation times, and diffusion coefficients in polymers and gels, foods, and materials (43–47). One key attribute of single-sided MR systems is the open access to the sample they provide, a feature we exploit in our design, in which a fluorescence optical microscope with long-working distance objective was installed above the biological specimen to image simultaneously intracellular  $\text{Ca}^{2+}$  transients. Fluorometric  $\text{Ca}^{2+}$  imaging detects caged or bound  $\text{Ca}^{2+}$  ions released during neuronal activity and represents a direct method for detecting neuronal activity (48,49).

In this study, we performed experiments on the organotypic cultures of rat cortex, which have been widely used in neuroscience as a biological model of neuronal activity (50–54) and in MRI studies (11,28,55). Organotypic cortical cultures largely maintain the *in vivo* cortical cytoarchitecture including cortical layers and cortical cell types, which can be grown and recorded for several weeks in the incubator (51,52). More importantly,

organotypic cultures *in vitro* display bursts of spontaneous neuronal activity, so-called up- and down-states, that is similar to *in vivo* nervous tissue (53,56,57). Thus, no pharmacological manipulation is required to initiate neuronal activity, and the culture remains in a long-term homeostatic state while exhibiting large transients of neuronal activity (54). Organotypic cultures do not contain a cerebrovascular system and thus are free of artifacts of hemodynamic origin, such as pulsation and flow artifacts or artifacts associated with respiration and variable oxygenation, which are known confounds in fMRI studies *in vivo*.

In this work, we focus on the description and demonstration of this test bed to assess the direct fMRI measurement of neuronal activity. This article is organized as follows: A systematic description of each essential component of the test bed, which consists of the organotypic cortical culture, the MR system, the fluorescence calcium imaging, etc., is provided. After that, the performance of the system, in particular, the properties and stability of the MR and fluorescence calcium signals is described. Then, the results of the experiments with simultaneous calcium fluorescence imaging and a conventional MR multi-echo pulse sequence without imaging are analyzed and discussed. Finally, the benefits and limitations of such a testing system and its potential applications for future work are discussed.

## MATERIALS AND METHODS

### Organotypic rat-cortical culture

For the preparation of organotypic tissue cultures, the somatosensory cortex was taken from acute coronal slices of newborn rats (postnatal day 0–2, Sprague–Dawley). Organotypic cultures made from coronal slices maintain the layered organization of the cortex and the parallel orientation of pyramidal neurons with respect to each other. The acute slices (350  $\mu\text{m}$  thickness) were attached to the no. 1 coverslips by using a plasma-thrombin mixture, and submerged in 800  $\mu\text{L}$  of culture medium and incubated at  $35.0 \pm 0.5$  °C. The medium was replaced every 3–4 days. The tissue was cultured for 2–3 weeks, when the tissue thickness became approximately 100–200  $\mu\text{m}$ . More details about growing this type of organotypic culture can be found in (54,58). We commonly mounted two cortical slices close together on each coverslip to increase tissue volume within the RF coil. This approach allowed the neuronal cultures to preserve most of the architectural specificity of a cortical network.

### Setup for simultaneous calcium fluorescence imaging and functional MR

Figure 1 is a schematic diagram, showing the placement of the MR and fluorescence imaging systems with respect to the *in vitro* specimen. Organotypic cultures from rat cortex were kept in a custom-machined environmental chamber to maintain the culture's vitality during the experiment and to allow for perturbation of environmental conditions. The chamber was mounted on the top of a single-sided MR system with permanent magnets; this MR system provided open access to the tissue culture. An RF surface coil was attached directly below the coverslips to transmit and receive MR signals. An optical fluorescence microscope was mounted above the MR stage, thus enabling calcium imaging down onto the organotypic culture. One advantage of this optical system is its long working distance objectives (87 mm with the 0.63 $\times$  lens), which separates the permanent magnets

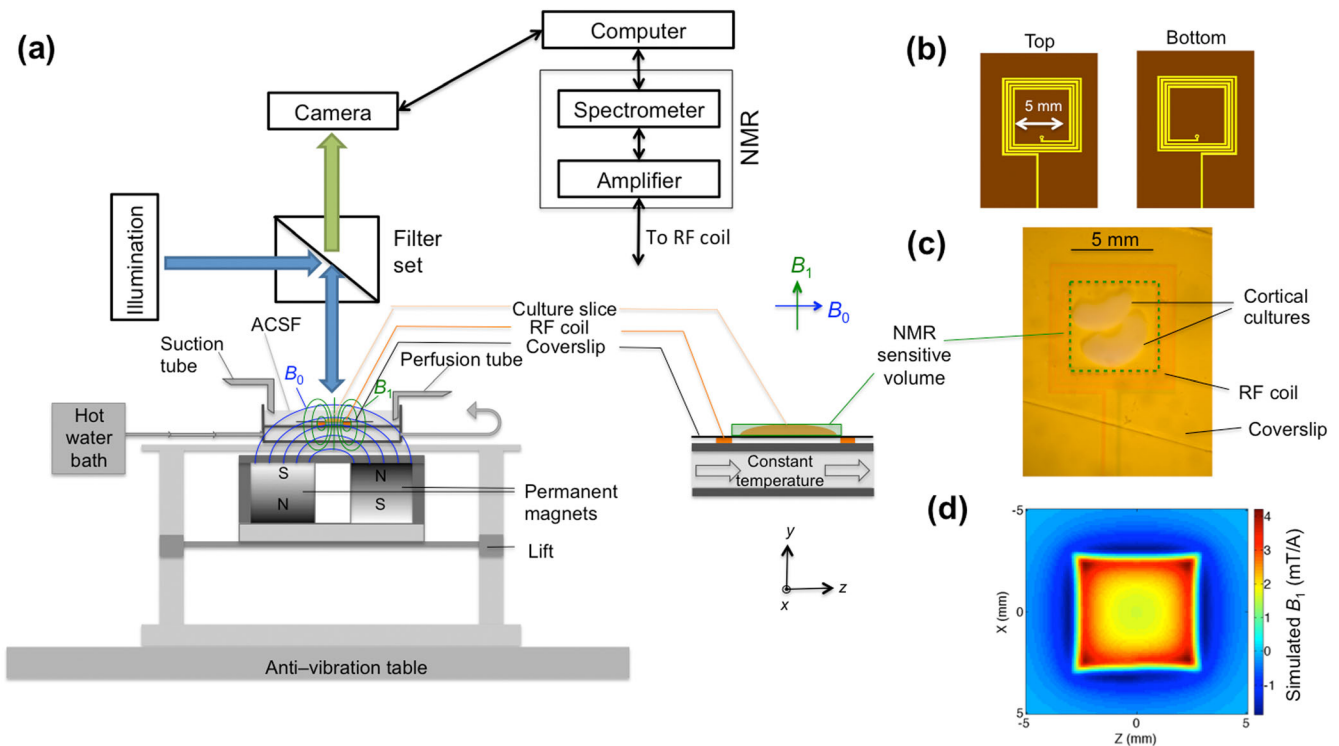


**Figure 1.** Setup for simultaneous functional MR and calcium imaging. (a) Schematic diagram of the simultaneous MR and fluorescence imaging test bed (left) and an enlargement of the components near the organotypic cultured tissue (right), which is immersed in artificial cerebral spinal fluid (ACSF). (b) Top and bottom layers of the two-layer multi-turn RF surface coil. (c) A real image of the coil with the cortical culture mounted under 0.63× magnification. (d) A simulated 2D  $B_1$  field distribution at  $y = 0.2$  mm in the  $x$ - $z$  plane.

and the fluorescence microscope. Another advantage is its large field of view (FOV) ( $8.8 \times 6.6$  mm at 1× magnification), which can capture the entire tissue specimen ( $\sim 2 \times 4$  mm for each cortex). The details of each part of this test bed are described in the following sections.

### Fluorescence microscope

A macro-zoom fluorescence microscope (MVX10 MacroView; Olympus Inc., Center Valley, PA, USA) was modified and mounted on an optical table using a custom machined stainless-steel stand and a boom. A 0.63× MVX Plan Apochromat lens (Olympus Inc., USA) with a 0.15 numerical aperture (NA) was used with total magnification ranges from 0.63× to 12.6×. A 100W Mercury Apo lamp housing and transformer were used as a light source. A color CCD camera (ProgRes® CF scan, Jenoptik, Inc., Jena, Germany) with high frame rates (51 fps for  $680 \times 512$  pixels) was mounted on the microscope for fast fluorescence imaging.

### Calcium staining and imaging

Vital calcium imaging was achieved using 50  $\mu$ M Oregon Green 488 BAPTA-1 (OGB; Life Technologies, NY, USA). OGB was dissolved in 10  $\mu$ L pluronic F-127 (20% in DMSO; Life Technologies) and 790  $\mu$ L freshly prepared artificial cerebrospinal fluid (ACSF). The ACSF consists of 124 mM NaCl, 3.5 mM KCl, 10 mM glucose, 26.2 mM  $\text{NaHCO}_3$ , 0.3 mM  $\text{NaH}_2\text{PO}_4$ , 2.4 mM  $\text{CaCl}_2$  and 2 mM  $\text{MgSO}_4$ . Cultures were incubated for 45–90 min in a roller tube incubator and washed in ACSF for 20–60 min before imaging. Calcium images were acquired with GFP fluorescence filter units from Olympus (Olympus America Inc., Center Valley, PA, USA),

whose excitation, dichroic, and emission lengths are 450–490 nm, reflection < 495 nm, and 500–550 nm, respectively. The real-time calcium imaging was acquired using ProgRes® CapturePro v2.8.8 software (Jenoptik, Inc., Jena, Germany).

### Single-sided MR system

The permanent magnets of the single-sided MR system (NMR - MOUSE) were purchased from Magritek European, Aachen, Germany. A Kea spectrometer and Prospa acquisition software (Magritek, Inc., Wellington, New Zealand) were used to generate and collect the MR signal. Both the MR system and the optical microscope were mounted on an antivibration optical table to eliminate spurious mechanical vibrations. The single-sided MR system with four permanent magnets mounted in an iron yoke [Fig. 1, see reference (44) for details] generates a relatively uniform magnetic field (0.32 T,  $\sim 15 \times 15$  mm) in the  $x$ - $z$  plane at  $\sim 15$  mm from the surface of the magnets. In this NMR system, the thickness of the selective slice is set by controlling the acquisition time ( $T_{\text{acq}}$ ) rather than setting the RF pulse length ( $T_{\text{RF}}$ ) as in conventional MRI. Generally, we used a short, hard RF pulse ( $T_{\text{RF}} \sim 8$   $\mu$ s) to excite a slice of sample with a thickness ( $\Delta y_{\text{RF}}$ ) of  $\sim 200$   $\mu$ m:

$$\Delta y_{\text{RF}} = 2\pi / G_0 T_{\text{RF}} \quad [1]$$

where  $G_0 = 650$  kHz/mm is the strength of the uniform magnetic field gradient across the selective volume in the  $y$ -direction. Then the MR signal was acquired and integrated in  $T_{\text{acq}}$  ( $T_{\text{acq}} \geq T_{\text{RF}}$ ); in this way, the integrated MR signal only selects the spins with resonance frequencies in the acquisition bandwidth to achieve the desired slice thickness  $\Delta y$  that is also defined with Equation 1 with  $T_{\text{RF}}$  replaced by  $T_{\text{acq}}$  (42,43).

To reduce the MR FOV in the  $x$ - $z$  plane so that it matched the tissue's dimensions, a homemade two-layer multi-turn micro RF surface coil (Fig. 1) was used with an inner dimension (5 mm) approximately the size of two cortical slices. The two-layered multi-turn RF surface coils (Fig. 1) were fabricated by SF Circuits Inc., San Mateo, CA, USA. On each side of the 225- $\mu\text{m}$  thick polyimide board, there were four turns of copper conductors with 18- $\mu\text{m}$  height, 200- $\mu\text{m}$  width, and a lateral spacing of 50  $\mu\text{m}$ . The top layer and the bottom layer (Fig. 1b) were connected by a copper hole. A calculation based on the Biot-Savart law was performed to simulate the  $B_1$  field distribution produced by the RF coil; this simulation can provide a good estimate of the ground truth at these low frequencies.

**MR pulse sequences**

The Carr-Purcell-Meiboom-Gill (CPMG) pulse sequence (Fig. 2a) is widely used in single-sided MR applications to measure the effective transverse relaxation time,  $T_{2\text{eff}}$ , which is affected by both the transverse relaxation time,  $T_2$ , and the self-diffusion coefficient,  $D$ , in the presence of a static field gradient,  $G_0$  (42):

$$\frac{1}{T_{2\text{eff}}} = \frac{1}{T_2} + \frac{1}{3}(\gamma G_0 \tau)^2 D \alpha \quad [2]$$

where  $\gamma$  is the gyromagnetic ratio of protons,  $\tau$  is half the echo time, and  $\alpha = 1.32$  (59). The sensitivity of the  $T_{2\text{eff}}$  to  $T_2$  and  $D$  was examined with a series of manganese chloride ( $\text{MnCl}_2$ ) solutions while  $\tau$  was adjusted (59).

A well-known feature of diffusion MRI in the cortex is the multi-exponential behavior of the diffusion signal, which is often modeled by a four-parameter biexponential function (7,9,25,31,60,61):

$$S(b) = S_0[(1 - f_{\text{slow}})\exp(-bD_{\text{fast}}) + f_{\text{slow}}\exp(-bD_{\text{slow}})] \quad [3]$$

where  $S$  is the diffusion MR signal and  $S_0$  is the MR signal without diffusion weighting;  $b$  is the diffusion weighting;  $D_{\text{fast}}$  and  $D_{\text{slow}}$

are the fast and slow diffusion coefficients, respectively; and  $f_{\text{slow}}$  is the slow diffusion compartment fraction. To measure the water diffusion, we used a spin echo (SE) in the presence of a static magnetic gradient (Fig. 2b). CPMG echo trains were acquired and summed after the main diffusion-weighting period to improve sensitivity. In this pulse sequence, the  $b$  value is defined as (44):

$$b = \frac{2}{3}(\gamma G_0 \tau_1)^2 \tau_1 \quad [4]$$

where  $\tau_1$  is the half echo time of the first spin echo for diffusion encoding.

**Experimental protocol**

Before experiments were performed, the organotypic cultures were moved from the roller incubator to the custom chamber (Fig. 1) after the calcium dyes were loaded. During experiments, the cultures were continuously perfused with oxygenated ACSF (95%  $\text{O}_2$  and 5%  $\text{CO}_2$ ), and the temperature of the perfusate was kept constant with an inline temperature controller. A water bath, attached to the bottom of the chamber, was used to control precisely the temperature inside the chamber. Water from a large water bath outside the experimental stage circulated through this bath and kept it at a constant temperature. A fiber-optic temperature sensor (OpSens TempSens, OpSens Inc., Quebec, Canada) was mounted near the tissues to monitor their temperature during the experiments. The temperature was kept at  $34.2 \pm 1.0$  °C during experiments, and the temperature gradient inside the RF coil was less than 0.5 °C. Of the 17 samples scanned, 14 samples were statistically analyzed, and three were rejected because of failure in temperature maintenance or MR acquisition instability.

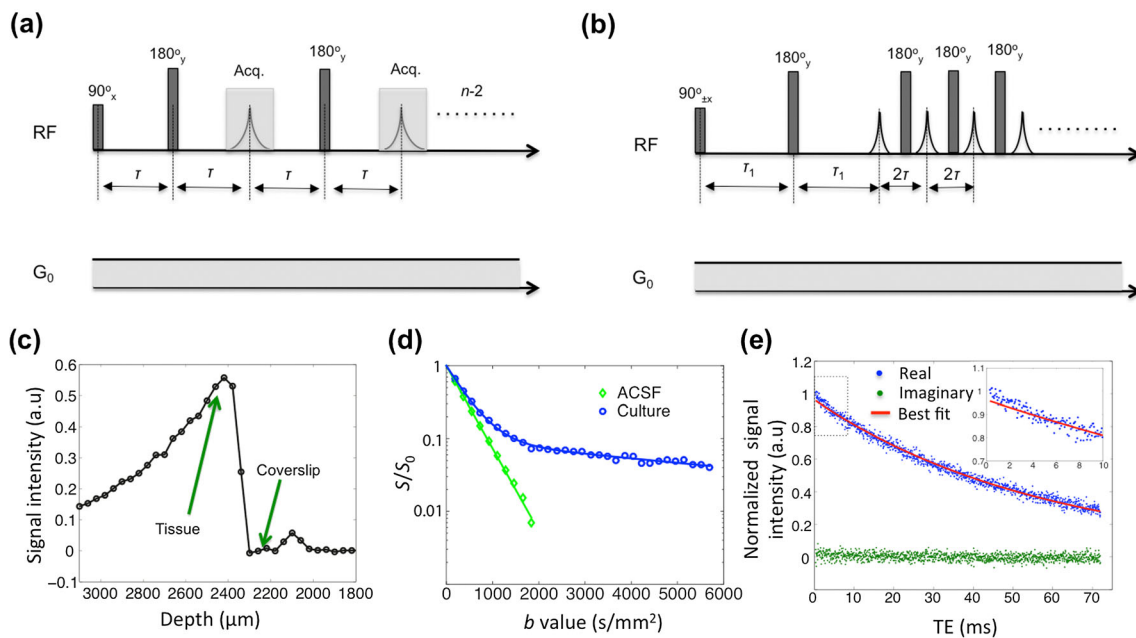


**Figure 2.** MR pulse sequences and signals. Diagrams of the two pulse sequences: (a) Carr-Purcell-Meiboom-Gill (CPMG) and (b) diffusion editing SE with CPMG detection. (c) MR spatial localization of the culture sample. (d) The diffusion-weighted MR signal of ACSF (green) and the culture sample (blue) in which the continuous curves are the fitting results with models. (e) One example of the CPMG signal of the culture in which the continuous red curves are the fitting result with a single-exponential function. The subplot in the middle is the enlargement of the dashed red box.

### MR spatial localization

After the organotypic cultures had been mounted in the chamber, a 1D profile with 40- $\mu\text{m}$  resolution was obtained to determine the position of the tissue. A 1D spatial profile in the  $y$ -direction was achieved by mechanically raising and lowering the magnet with a precision lift (best resolution  $\sim 10 \mu\text{m}$ ) and the CPMG pulse sequence with matching slice-selective acquisition (Eq. 1). The parameters for the CPMG sequence were: TR = 2 s, 500 echoes with  $\tau = 40 \mu\text{s}$ , and 8 repetitions. The signal intensity was defined as the average of the 500 echoes to improve the signal-to-noise ratio (SNR). In this process, the positions of the RF coil, the chamber, and the cultures were fixed while only the selective volume was raised and lowered as the magnet was moved up and down. First, the coverslip was found (Fig. 2c), and then the magnet was moved up 80–120  $\mu\text{m}$  to locate the middle of the tissue.

### Diffusion MR measurements

After a central slice covering the middle portion of the tissue was identified, the SE pulse sequence was performed with 32  $b$  values ranging from 0 to 5700  $\text{s}/\text{mm}^2$  with a step of 184  $\text{s}/\text{mm}^2$ . The other parameters were: TR 4 s, 4000 echoes in the CPMG with  $\tau = 20 \mu\text{s}$ , and 8 repetitions with a two-step phase cycling (Fig. 2b). The acquisition time in each echo was 16  $\mu\text{s}$  with 32 sampling points, resulting in a thickness of the selective volume of  $\sim 100 \mu\text{m}$ .

### Simultaneous calcium fluorescence imaging and MR recording

In the MR, the CPMG pulse sequence was used for fast recording: TR = 1 s and 1200 echoes with  $\tau = 30 \mu\text{s}$ . The acquisition time and the corresponding thickness of the selective volume were 16  $\mu\text{s}$  (32 sampling points) and 100  $\mu\text{m}$ , respectively. At the beginning of each experimental session, the phase of the CPMG signal was automatically adjusted to put the entire signal into the real channel. Calcium imaging was acquired with 1 $\times$  magnification, 8.8  $\times$  6.6 mm FOV, 680  $\times$  512 pixels, 100 ms exposure, and 10 frames per second. The focal plane and light intensity were adjusted at the beginning of each experiment and kept constant during the entire experiment session. The light intensity was adjusted to the minimal level that still enables one to distinguish neuronal activity from background noise to avoid strong photo bleaching and phototoxicity. During the experiments, both the camera frame time and the time of MR pulses (first 90° in the CPMG) were recorded with a precision of 1 ms. The total recording time range from 1 to 3 h, which were mainly restricted by the vitality of the culture with calcium staining and photobleaching.

### Signal processing and data analysis

All signal processing and analysis routines were implemented in MATLAB.

### Calcium signal processing

Regions of interest (ROIs) were manually selected on the two cortical slices (Fig. 3a) to show the spontaneous activity within and between the cultures. A background ROI was also manually selected close to the tissue but with no tissue inside. Comparison and correlation test of the calcium signal with the MR signal were performed by manually choosing a large ROI containing

all the tissues inside the RF coil. Background subtraction was further performed on the fluorescence signal from the large ROI by automatically subtracting the background. The fluorescence values were then expressed as relative percentage changes from the baseline,  $\% \Delta F/F$ . Formally,  $\Delta F/F$  is defined as the change in fluorescence over the baseline:  $\Delta F/F = (F_{\text{ROI}} - F_{\text{ROI},0})/F_{\text{ROI},0}$ , where  $F_{\text{ROI}}$  and  $F_{\text{ROI},0}$  denote the background-corrected fluorescence intensities in the ROI and its baseline calculated from a 30-second sliding window to overcome photobleaching artifacts. To detect calcium transients in an automated manner, a deconvolution algorithm, based on the 1D-deconvolution algorithm in MATLAB, was developed and applied to the fluorescence signal,  $\% \Delta F/F$ . The convolution kernel consisted of two parts: a delta function for the fast rising phase and a slow decay curve back down to the noise floor. Fluorescence decay curves were carefully fitted after neuronal activity events. A threshold was set in the deconvolved data to enable robust detection of neuronal activity events.

### MR CPMG and SE signal

The first four echoes that have systematic artifacts in each CPMG echo train were automatically eliminated. The zero-order phase correction was automatically applied to all the CPMG echo trains in each experiment. As for the spontaneous MR and calcium recording, the first 10 CPMG echo trains at each long recording were automatically removed to eliminate the instability present before the steady state was reached. Three MR parameters were extracted from each CPMG echo train:  $I_0$ , the average of the first 5<sup>th</sup> to 100<sup>th</sup> echoes [real channel, mean echo time (mTE) = 3.2 ms], denoted as the initial signal intensity;  $R$ , the weighting ratio between the average of the echoes from the 301<sup>st</sup> to the 1200<sup>th</sup> (real channel, mTE = 45.0 ms) and from the 5<sup>th</sup> to the 300<sup>th</sup> (real channel, mTE = 9.2 ms), denoted as the decay rate;  $\phi$ , the phase of the average of all the echoes, denoted as the phase of the MR signal.

In the case of the MR SE signal, the average of the entire CPMG echo train was used as the signal intensity at each  $b$  value. A trust-region-reflective nonlinear least square algorithm in MATLAB was used for model fitting.

### Effects of neuronal activity in the MR signal

The potential effects of neuronal activity on the MR signal were tested by binning the MR signal itself into two categories: active and resting states, based on its relative temporal location to each neuronal activity event. Then, paired comparisons were performed on each active MR waveform with its corresponding resting MR waveform by subtracting each active MR signal from its corresponding resting signal.

Two types of time-series analysis were performed. For type 1 we hypothesized that each neuronal activity event only affects the MR signal recorded after each neuronal activity event in a time window  $T$ , which ranges from 0.1 s to 1.0 s with a step of 0.1 s. The corresponding resting MR for each active MR was the MR recording the closest in time to the moment before the neuronal activity event (Fig. 5a). The fluorescence signal for each MR signal was the average of the entire deconvoluted fluorescence signal within  $T$  prior to each MR recording. For type 2 we hypothesized that each neuronal activity event only affects the MR signal recorded within 2 s before and following each neuronal event. All MR signals outside this 4-s time window were denoted

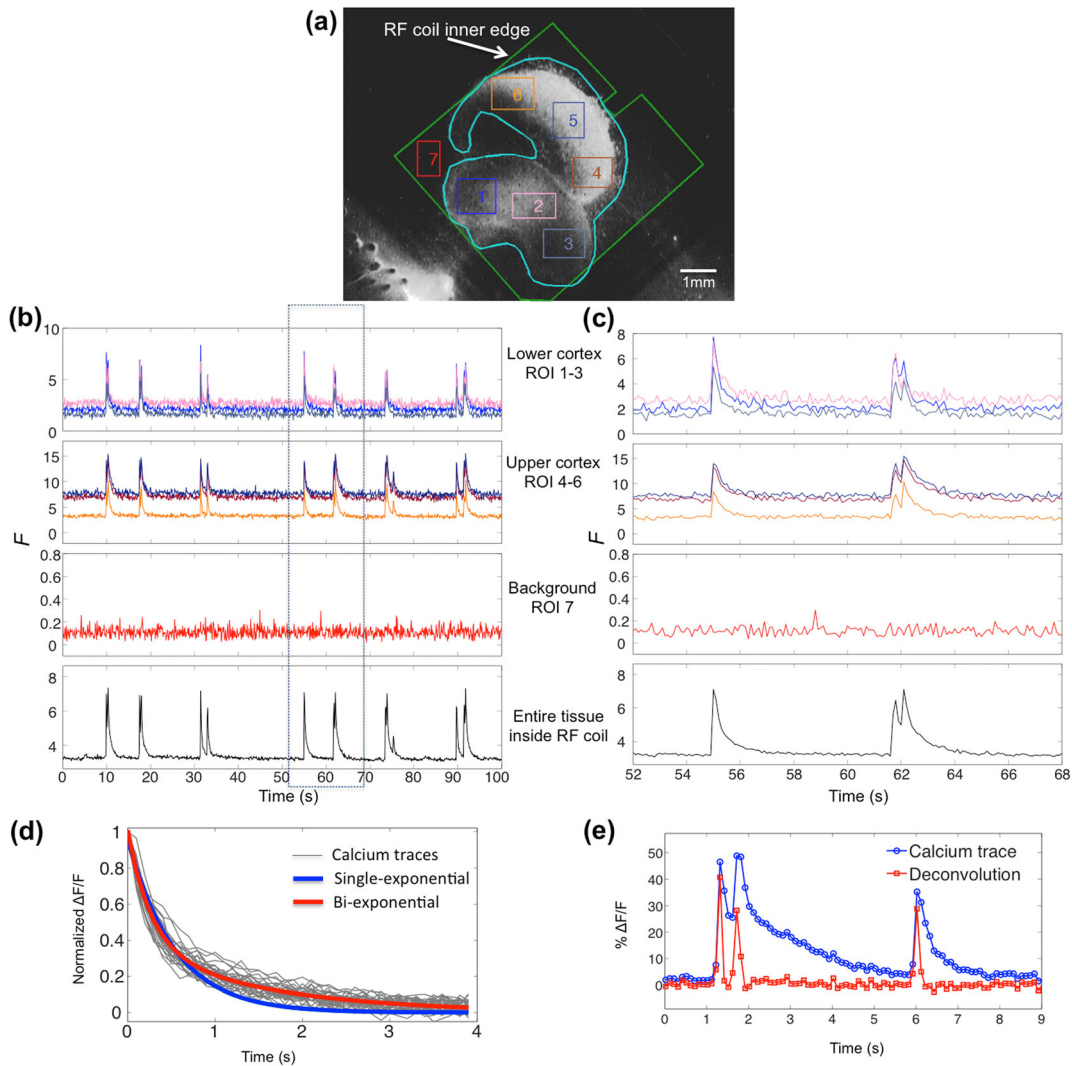


**Figure 3.** Spontaneous neuronal activity in the organotypic culture. (a) Fluorescence image of the organotypic cortical cultures (two coronal slices cocultured) and the position of seven different regions of interest (ROIs). (b) The raw calcium traces of each ROI in a 100-s time window. (c) The zoomed version of the selected box in (b). (d) The decay curves after each event and their fittings with single- and bi-exponential functions. (e) Example of the deconvolution algorithm on the calcium signals.

as resting state (Fig. 5b). The fluorescence signal for each MR signal was the average of the entire deconvoluted fluorescence signal within 2 s before and following each MR recording. To scale the difference across samples and perform statistics, the fluorescence signals for all MR recordings in each sample were normalized by their maximum value in the active state. Each active MR was further binned into different groups on the basis of how distant it was in time ( $\Delta$ ) from the neuronal activity event with a time step 0.2 s. For each active MR, the four resting MRs closest to it in time, both before and after, were chosen and averaged as the corresponding resting MR.

### Immunohistochemistry and confocal imaging

A subset of cultures was used for immunological identification of cell types. Cultures were rinsed in phosphate-buffered saline (PBS), fixed in 4% paraformaldehyde for 40–60 min, and incubated for 2 h at room temperature in blocking solution (10% normal donkey serum, 0.5% bovine serum albumin, and 1% Triton X-100 in PBS). The cultures were incubated in three primary

antibodies simultaneously at 4°C overnight in a carrier solution consisting of 1% normal donkey serum, 0.5% bovine serum albumin, and 0.3% Triton X-100 in PBS: (i) mouse anti-NeuN (EMD Millipore, Temecula, CA, USA; 1:1000); (ii) rabbit anti-s100 $\beta$  /anti-GFAP combined (Dako, Carpinteria, CA, USA; 1:2000 and 1:1000, respectively); and (iii) goat anti-Iba1 (Abcam, Cambridge, MA, USA; 1:500). After the cultures were washed for 5, 15, and 5 min in PBS containing 1% normal donkey serum and 0.3% Triton X-100, they were incubated for 1 h at room temperature in secondary antibodies, diluted in carrier solution: Alexa 555 donkey anti-mouse; Alexa 488 donkey anti-rabbit, Alexa 633 donkey anti-goat (1:1000, Invitrogen, NY, USA). The cultures were then washed two more times with the wash solution for 5 and 15 min at room temperature. Before imaging, cultures were rinsed in PBS for 5 min and mounted on coverslips with a fluorescence-preserving mounting medium (MOWIOL 4–88, EMD Millipore, Temecula, CA, USA). Control images of cortical cell distribution were obtained with an 8-day-old rat brain fixed by transcardial perfusion. Brain slices (200  $\mu$ m thick) from the same cortical region as the organotypic cultures were immunostained following the same

procedure as described above. Confocal images were obtained on an inverted Zeiss LSM 510 with a 20x Zeiss plan-apochromatic objective (0.75NA) at the Microscopy and Imaging Core Facility, NICHD, NIH.

## RESULTS

### Micro RF coils

Tuning and matching the coil with an external circuit were achieved with a quality factor (Q) of 14 (62). The  $B_1$  field distribution in the selective plane (middle of the tissue,  $y \sim 200 \mu\text{m}$ ) shows a plateau inside the RF coil with maximal sensitivity combined with a slight rise near the inner edge of the coil and a rapid decay starting at the inner edge of the coil in the lateral directions (Fig. 1d).

### MR spatial localization

In the 1D profile (Fig. 2c), the signal intensity increased as the selective volume was lowered toward the surface of the RF coil, but the signal dropped quickly to zero as the selective volume moved onto the coverslips (thickness  $\sim 0.13 \text{ mm}$  to  $0.16 \text{ mm}$ ). Then, the magnet was moved up by  $80 \mu\text{m}$  to  $120 \mu\text{m}$  to locate the center of the culture tissues.

### MR diffusion measurements

To confirm that the selective volume (selective thickness  $\sim 100 \mu\text{m}$ ) contained the tissue, diffusion MR was performed prior to the simultaneous fluorescence and MR recording (Fig. 2d). The diffusion decay signals were fit well by a biexponential function with the tissue in place. In contrast, the diffusion MR signal of the ACSF itself showed a clear single-exponential decay. Statistics for the 14 samples and the 5 ACSF samples are shown in Table 1.

### Simultaneous calcium fluorescence and MR recording

One example MR CPMG signal (3000 averages) from one sample is shown in Fig. 2e. Most of the signal intensity is in the real channel after the phase has been automatically adjusted (imaginary/real ratio is less than 0.1%). The decay curves in all the samples ( $n = 14$ ) were fit well by a single-exponential function with  $T_{2\text{eff}} = 59.0 \pm 2.7 \text{ ms}$ , except for the faster decaying part at echo time (TE)  $< 5 \text{ ms}$  with a fraction  $2.5\% \pm 0.8\%$  and relaxation time  $< 10 \text{ ms}$ . As for the control with ACSF alone ( $n = 6$ ), the decay curves were fit well by the single-exponential function over the entire TE range with  $T_{2\text{eff}} = 56.1 \pm 0.3 \text{ ms}$ , which is slightly (but significantly,  $p < 0.001$ ) smaller than the results of the cultures. The small, faster-decaying parts in the culture slices might arise from some highly ordered water molecules (such as macromolecule-bound water) and some macromolecules (such as metabolites and proteins).

In the calcium images, three ROIs were selected in each cortex region (ROI 1–6), and one ROI (ROI 7) close to the RF coil inner edge but not containing tissue was selected as background. Highly spontaneous activity was observed in all six ROIs, 1–6, (Fig. 3b, 3c), whereas the background ROI 7 showed low fluorescence intensity without neuronal activity information. The correlation coefficients of the fluorescence signals (30-min recording) between all ROI's, 1–6, were no less than 0.78. The fluorescence from the large ROI containing the entire tissue inside the RF coil also showed high correlation coefficients ( $\geq 0.88$ , Table 2) with all ROIs in the two cortex region, which makes it representative of the calcium signal there and therefore it was used for further correlation tests with the MR signals.

Figure 3d shows 30 decay curves after neuronal activity from one experiment (solid gray lines). A biexponential function can fit the averaged decay curve very well with a fast decay component ( $69 \pm 11\%$ ) and a slow decay component, with time constants (the time required for the signal to decay to  $1/e$ )  $0.21 \pm 0.07 \text{ s}$  and  $1.67 \pm 0.37 \text{ s}$ , respectively. The failure of the single-exponential fit might be a result of the large-scale imaging in which the calcium kinetics depends on local calcium concentration, neuron types, and the location of the neurons (63,64). By implementing the biexponential decay function into the convolution kernel, our deconvolution algorithm can precisely and successfully detect the time and amplitude of each neuronal activity (Fig. 3e).

### Stability of the MR and calcium recording

An example of a 1.5-h simultaneous calcium and MR recording is displayed in Fig. 4. For a healthy culture sample, good neuronal activity can last from one to several hours under continuous optical and MR recording. In this example, the neuronal activity was quite stable during the entire 1.5-h recording. At the same time, the MR signal, which includes all three parameters ( $I_0, R, \phi$ ) extracted from each CPMG echo train, was also very stable.

**Table 2.** Correlation coefficient table for the calcium signals from each region of interest (ROI) on the two cultures (Fig. 3) and the entire tissue inside the RF coil

ROI	1	2	3	4	5	6	Entire tissue
1	1.00	0.85	0.89	0.85	0.83	0.85	0.92
2	0.85	1.00	0.82	0.81	0.80	0.81	0.88
3	0.89	0.82	1.00	0.80	0.78	0.81	0.88
4	0.85	0.81	0.80	1.00	0.93	0.93	0.96
5	0.83	0.80	0.78	0.93	1.00	0.93	0.95
6	0.85	0.81	0.81	0.93	0.93	1.00	0.96
Entire tissue	0.92	0.88	0.88	0.96	0.95	0.96	1.00

**Table 1.** Diffusion parameter estimation with the bi-exponential model for the organotypic cultures and with the single-exponential model for the ACSF

Organotypic cortical culture samples ( $n = 14$ )					
$D_{\text{fast}} (10^{-3} \text{ mm}^2/\text{s})$	$2.56 \pm 0.05$	$D_{\text{slow}} (10^{-3} \text{ mm}^2/\text{s})$	$0.16 \pm 0.03$	$f_{\text{slow}}$	$10.3 \pm 3.1\%$
ACSF ( $n = 5$ )					
$D (10^{-3} \text{ mm}^2/\text{s})$	$2.66 \pm 0.01$				

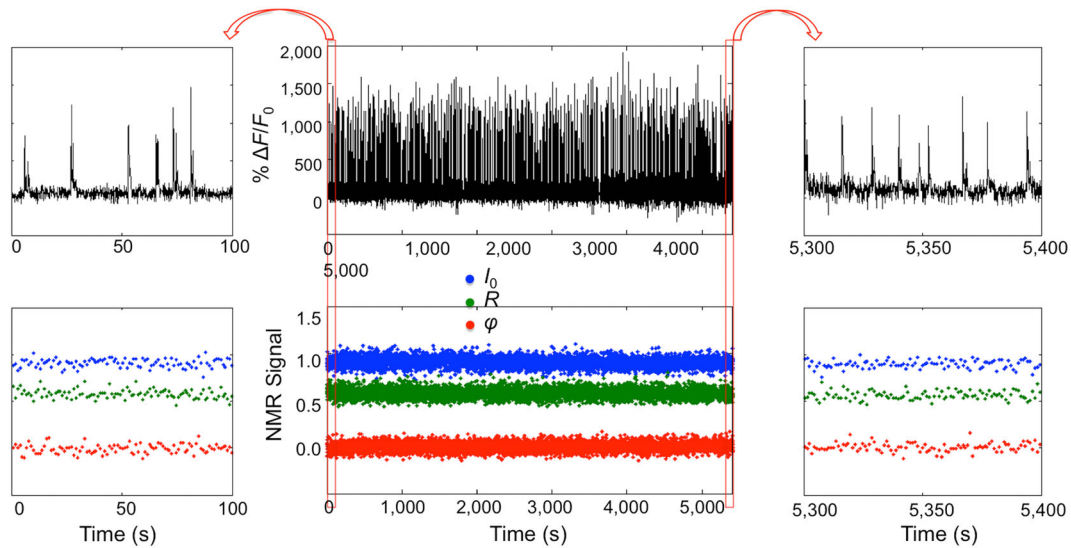


**Figure 4.** Stability of the MR and fluorescence signal. Simultaneous MR (bottom, three MR parameters) and calcium fluorescence (top) recording from one culture sample for ~1.5 h. The first and last 100 s were expanded and are shown on the left and right sides of the central panel. Visual inspection does not reveal any correlations between the two.

In the above example, the signal-to-noise ratio (SNR) for  $I_0$  and  $R$  are 12.9 and 15.0, respectively, and the standard deviation of  $\varphi$  is 0.04 rad [ $\sim 6 \times 10^{-3}$  parts per million (ppm) in frequency]; similar noise levels were found in all admissible experiments and in two control experiments in which only ACSF was present. In some experiments, there was low-frequency ( $<0.005$  Hz) drift, which might be caused by small trapped air bubbles in the ACSF line, slow motion caused by temperature bending of the coverslips, etc. The drift of  $I_0$ ,  $R$ , and  $\varphi$  in the 1.5-h recording session was less than 2.6%, 0.7%, and 0.02 rad ( $\sim 3 \times 10^{-3}$  ppm), respectively, for the example in Fig. 4 and 5.8%, 3.2%, and 0.09 rad, respectively, for all the samples used in our statistical analysis. However, this type of drift is small and can be neglected when active- and resting-state MR are compared in the data analysis procedure as that time window is less than 12 s.

#### Effects of neuronal activity in the MR signal

The potential effects of neuronal activity on the two MR parameters,  $I_0$  and  $R$ , were further analyzed. In the Type 1 analysis, Student's  $t$ -tests were performed on the results from all the admissible cultures with the null hypothesis that the mean of the difference between active and resting MR was equal to 0. No significant changes were observed for any of the two MR parameters ( $I_0$  and  $R$ ) for the time window  $T$  from 0.1 s to 1.0 s ( $p \geq 0.14$  for all of the tests, Fig. 5e), whereas the calcium signal showed much higher intensity in the active state (Fig. 5c). For the Type 2 analysis, similar Student's  $t$ -tests were performed on the paired comparison between the active (the entire 4-s time window without further binning) and resting MR signals, and no significant changes were observed for the two parameters either ( $P \geq 0.37$ , Fig. 5d). The time profiles of the changes of the MR parameters are shown in Fig. 5f. All of the averaged changes of the two MR parameters ( $I_0$  and  $R$ ) from all of the admitted cultures were less than 0.5% and 0.4%, respectively. One-way ANOVA performed on the time-profile MR results and the null hypothesis that the mean of the difference between active and resting MR in each bin were equal was also accepted ( $p = 0.85$  and 0.97 for  $I_0$  and  $R$ , respectively).

#### Immunohistochemistry

To clarify the cell types and densities in the organotypic culture, immunohistochemistry was performed using three antibodies, which label neurons, astrocytes and microglial cells with three different colors. In the control (acute rat brain cortex slices, Fig. 6a), all three types of cells were spatially homogeneously distributed with the neuron as the dominant cell type. In the organotypic culture, a layer of astrocytes formed at the surface (Fig. 6b) and border of the culture (Fig. 6c,d) whereas the more susceptible neurons were predominantly found deeper in the core of the culture ( $>10 \mu\text{m}$ , Fig. 6c,d). Visual inspection indicates even higher cell density of neurons at these steps than at the one in the control.

#### DISCUSSION

Here we provide a novel, versatile, and stable test bed for non-BOLD fMRI assessment consisting of (i) a well-established biological model of neuronal activity, (ii) a well-controlled environmental chamber to maintain stable neuronal activity and (iii) a multimodal optical and MR means of recording neuronal activity. In our design, real-time calcium images can be acquired simultaneously with the MR signal. Calcium imaging is a well-established method for quantitatively measuring neuronal activity (63,64). This setup allows for direct comparison of the MR signals and the calcium-based indicators of neuronal activity and precise temporal localization of the effects of neuronal activity on MR signals.

The use of organotypic cortical cultures as a biological model of neuronal activity eliminates any possible hemodynamic contributions to the MR signal. The organotypic cultures possess healthy neurons similar to those in the *in vivo* cortex with high cell densities and extracellular matrix (51). Moreover, spontaneous activity in organotypic cortex cultures organizes as neuronal avalanches (53), a common dynamic mode of ongoing activity also observed *in vivo* in humans and nonhuman primates (56,57). Together, the high neuronal density and synchronized neuronal activity provide the best chance to

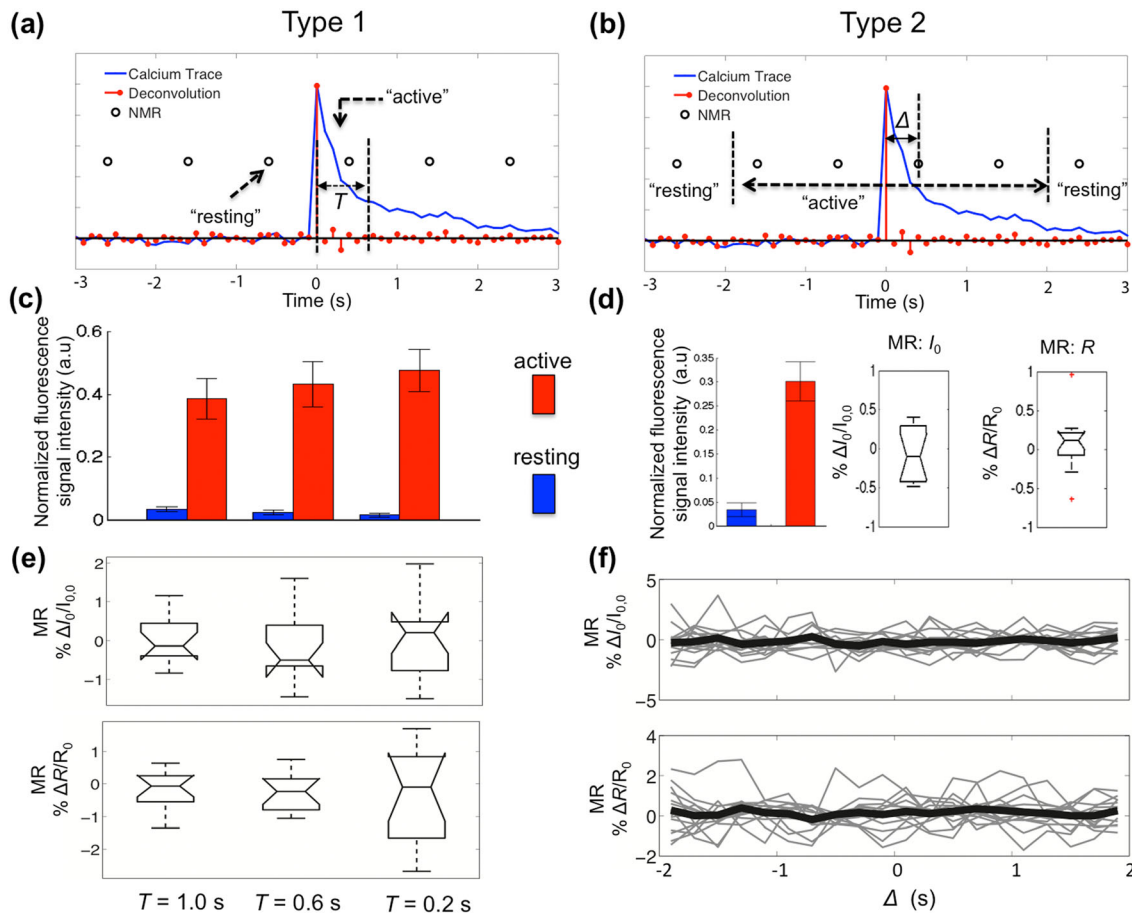


**Figure 5.** Two types of statistical methods for analysis of the potential effects of neuronal activity on the MR signal. Schematic diagram of the analysis methods: Type 1 (a) and Type 2 (b). For Type 1, bar plots of the deconvoluted fluorescence signal and boxplots of statistical results of the paired-comparison MR in the active and resting state at time window  $T = 1.0$  s,  $0.6$  s, and  $0.2$  s are shown in (c) and (e). For Type 2, bar plots of the deconvoluted fluorescence signal and boxplots of statistical results of the paired-comparison MR in the entire active (4-s time window) and resting states are shown in (d). The time profiles of the group results for Type 2 analysis are shown in (f), in which the narrow gray curves are the averaged result from each culture, and the broad black line is the average of the 14 cultures.

observe changes in the MR signal due to neuronal activity, if such relationships exist.

Performing electrophysiology experiments inside the MRI magnet could be very technically challenging due to the electromagnetic interface (36,37). The closed configuration and the size of the magnet bore also make it difficult to move the modern optical microscope into inside the MRI scanner (38–41). Several hybrid setups with simultaneous optical recording and fMRI were reported, but they were limited to hemodynamic-based optical imaging (65,66) or a single fiber recording (6). Here we offer an alternate solution by using the single-sided MR system (42), which is open-access, low-cost, portable, reliable and compatible with high-resolution optical fluorescence imaging systems. Although in the MR spectroscopy experiment performed in this study an MR signal from the entire selective volume was used because MR imaging with single-sided MR system is currently too slow (42,67), the ultimate goal is to achieve simultaneous calcium and MR imaging. The fact that fast imaging techniques are under development for this system (68) suggests that the simultaneous MR and fluorescence imaging should be feasible in future.

An obvious question for this setup is whether the results from this experimental setup are relevant to conventional pre-clinical and clinical MRI systems, which normally have much higher

magnetic fields. Some MR contrasts, such as proton density, water self-diffusion, etc., are independent of the magnetic field strength, while others, such as the relaxation times, phase, Lorentz-force, etc., are dependent on the magnetic field strength (15,69–72). In principle, the changes in the non-field-dependent MR contrasts caused by neuronal activity observed here apply to a high magnetic field, while the other field-dependent changes should have a more careful discussion. For instance, the Lorentz-force effect can be several orders higher in the high magnetic field; therefore, the expected changes here should be several orders smaller. In addition, the inhomogeneous magnetic field also makes some pulse sequences used here different from those used in conventional MR and limits the application of some pulse sequences. For example, the gradient echo is unachievable in this system since the apparent relaxation time  $T_2^*$  is too short to detect (42), which is the common MRI sequence for phase imaging (11,73). What is more, the presence of the static gradient also puts limitations on the diffusion direction experiments. In addition, the baseline noise should also be considered in comparing the results from high-field MRI. For instance, the phase noise level (ppm) in our unshielded magnet is approximately 10 times higher than that observed in the high-field shielded MRI system (3,73). More detailed discussion will be provided for each specific MR contrast/sequence in our future work.

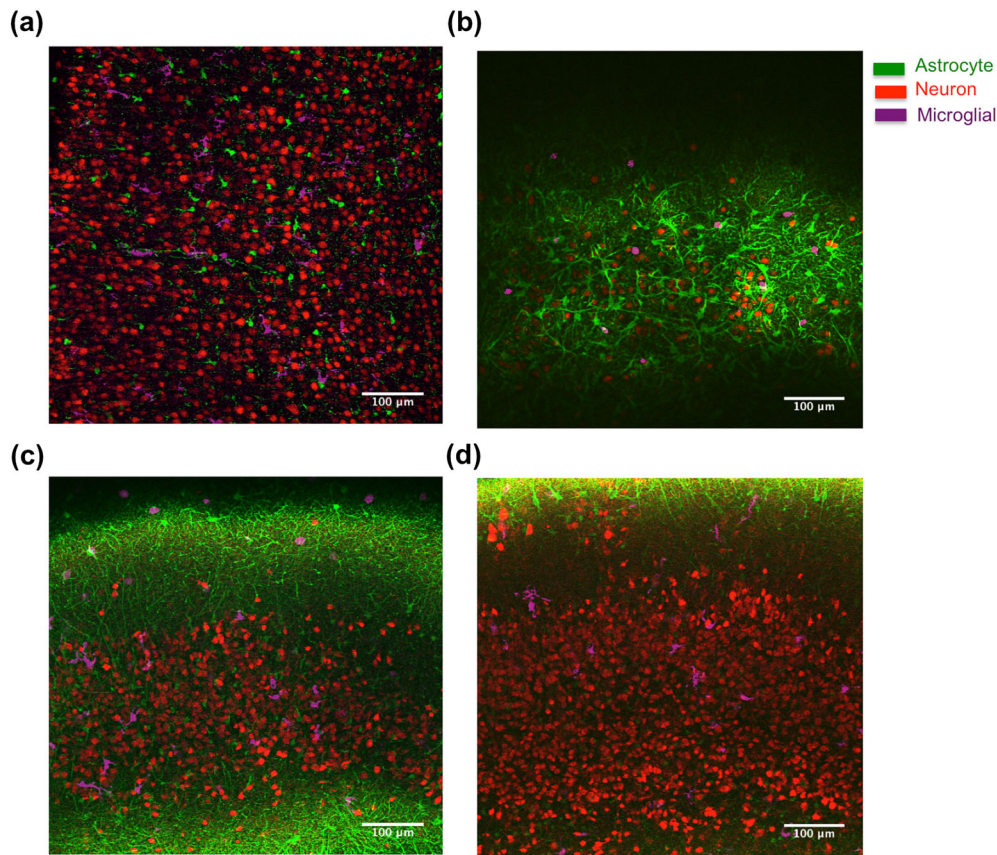


**Figure 6.** Fluorescence staining of rat brain slices with three antibodies labeled astrocytes, neurons, and microglial cells. (a) Control: acute brain slice from 8-day-old rat. (b–d) Organotypic cortical culture at different imaging depths (b, top layer; c, 10  $\mu\text{m}$  deep; d, 20  $\mu\text{m}$  deep).

While the SNR for a single MR echo train is not high (SNR  $\sim$  10–20 in this study) due to the low magnetic field and field inhomogeneity, here its sensitivity to the potential changes can be improved by multiple repetitions and prolonging our data recording. For example, in a 1-h experiment, there are approximately 180 active MR waveforms within a  $T = 0.5$  s time window after each neuronal activity if we assume the spontaneous neuronal activity occurs every 10 s. Taking the noise level in Fig. 5 and a statistical power of 0.80, the sensitivity of the detectable changes in this study will be 0.53% for  $I_0$  and 0.45% for  $R$ . Simultaneous recording on each sample can normally last no less than 1 h until some epileptic activity appears or normal activity disappears in the calcium imaging owing to phototoxicity. In the future, use of more neuronal-activity-sensitive and less toxic fluorescent dyes with low light intensity could result in an even longer recording time.

Because no imaging is performed in MR, partial volume is still a problem for MR detection in the current setup as the cultured tissue cannot occupy the entire MR selective volume, even when the selective volume was significantly reduced by the small custom RF coil (tissue occupies  $\sim$ 60% of the inner area of the coil). The non-single-exponential diffusion MR signal clearly demonstrated that the MR selective volume covers, at least partly, the two cultures inside the RF coil. From the results of the bi-exponential fitting,  $D_{\text{slow}}$  ( $0.16 \times 10^{-9}$   $\text{m}^2/\text{s}$ ) values obtained here are similar to those from *in vivo* rat brain and *in vitro* rat acute brain slices with imaging, while the  $D_{\text{fast}}$  ( $2.56 \times 10^{-9}$   $\text{m}^2/\text{s}$ ) values are larger and  $f_{\text{slow}}$  (10.3%) values are smaller than the corresponding values in the literature (9,25,27,74). The

differences are probably caused by the fast-diffusing ACSF in the selective volume being taken as the fast diffusion component in the bi-exponential fitting.

In this study, only a conventional CPMG MR pulse sequence was applied together with calcium imaging. The two parameters extracted from each CPMG echo train correspond to different and distinct contrast mechanisms.  $I_0$  is sensitive to the proton density and the longitudinal relaxation time  $T_1$  ( $\sim$ 1.5 s for the cultures). The weighting ratio,  $R$ , is sensitive to  $T_{2\text{eff}}$ , which depends both on the diffusion constant,  $D$ , and on the transverse relaxation time,  $T_2$ . In the culture, two diffusion components (fast and slow) were observed using the SE sequence. However, the associated  $T_2$  of each diffusion component and the exchange dynamics between these spin populations are still unknown and currently are beyond the scope of this article.

Statistical analysis of our results does not show statistically significant changes in the MR signals ( $I_0$  and  $R$ ) associated with neuronal activity when the active and the resting MR are compared, either by comparison of the MR signals before and after neuronal activity or inside and outside of the 4-s time window centered at the neuronal activity spike. However, it would be premature to conclude that this is a negative result for the newly proposed contrast mechanisms described in the Introduction (7,9,16), particularly as there are differences in the pulse sequences, the MR system, and the analysis methods used. As for the  $I_0$  effect, changes in proton density might be canceled out or masked by changes in  $T_1$ . In the case of  $R$ , a similar cancelation might occur between the contributions from  $D$  and  $T_2$ . Moreover, the diffusion time in this CPMG sequence is  $\tau = 30$   $\mu\text{s}$ , which is much

shorter than that in the conventional functional diffusion MRI experiments (~80 ms for clinical scanners and ~10–30 ms for pre-clinical scanners) (7–9,31,75). It has been reported that diffusion MR signals from the cortex are strongly dependent on diffusion time in the short diffusion time regime ( $\leq 10$  ms) (74,76).

More importantly, the biophysical basis of many aspects of neuronal activity is still poorly understood. MR visible effects may result from long-timescale changes, such as the BOLD fMRI signal ( $\geq 10$  s). In the organotypic cortical culture, spontaneous neuronal bursts occur approximately every 5 to 20 s. If the effect of the neuronal activity in the MR contrast lasted longer than that, the definition of the active and resting MR would need to be changed, as no resting state would exist in the entire recording. Moreover, if the effect of the neuronal activity in the MR contrast is on the millisecond range (77), our current setup might not have enough temporal resolution to capture this effect. More experiments are still needed to address these questions.

It is often presumed that it is sufficient to understand brain function by studying the distribution and pattern of neuronal activity while the role of astrocytes and other glial cells is often overlooked (78). This test bed, which uses healthy organotypic brain tissue, has the potential to be used not only to study neuronal excitatory behavior, but also to assess possible connections between MR signals and glial activity, particularly over a longer timescale than that used in these experiments. Though the current optical microscope does not have enough spatial resolution to distinguish glial cells from neurons, the fluorescence imaging of glial functions, e.g., astrocytes calcium signaling, can be achieved with proper glial-specific synthetic (79) or genetically encoded calcium fluorescence sensors (80). We view these applications as important future uses of this novel test system.

Although important information can be extracted from the CPMG echo trains, the main purpose of this paper is to describe and demonstrate the successful operation of this novel test bed. The clear biexponential diffusion signal in the SE pulse sequence shows that the MR selective volume covers the tissue on the coverslip. Figure 4 demonstrates the stability of both the calcium and MR signals during a long recording period. Two types of analysis methods were also provided to look for the potential effects of neuronal activity. It is important to note that because the pulse sequence design and experimental protocol are flexible to modify, it is possible to validate or test existing or newly proposed MR sequences and address open biophysical questions with this method.

## Acknowledgements

This work was supported by the Intramural Research Program (IRP) of the *Eunice Kennedy Shriver* National Institute of Child Health and Human Development (NICHD), NIH. Special thanks to Ms. Lynne A. Holtzclaw and Dr. James T. Russell from the Microscopy and Imaging Core (MIC) Facility at NICHD, NIH for assistance in immunohistochemistry and confocal imaging and Ms. L. Salak for editing the manuscript. We are also grateful to Dr. Alan P. Koretsky from the Laboratory of Functional and Molecular Imaging at the National Institute of Neurological Disorders and Stroke (NINDS) for useful discussion and the support from the IRP of NINDS.

## REFERENCES

1. Kwong KK, Belliveau JW, Chesler DA, Goldberg IE, Weisskoff RM, Poncelet BP, Kennedy DN, Hoppel BE, Cohen MS, Turner R. Dynamic

- magnetic resonance imaging of human brain activity during primary sensory stimulation. *Proc. Natl. Acad. Sci. USA.* 1992; 89: 5675–5679.
2. Ogawa S, Tank DW, Menon R, Ellermann JM, Kim SG, Merkle H, Ugurbil K. Intrinsic signal changes accompanying sensory stimulation: functional brain mapping with magnetic resonance imaging. *Proc. Natl. Acad. Sci.* 1992; 89: 5951–5955. DOI:10.1073/pnas.89.13.5951.
3. Scott G, Joy ML, Armstrong R, Henkelman R. Sensitivity of magnetic-resonance current-density imaging. *J. Magn. Reson.* 1992; 97: 235–254.
4. Logothetis NK. The ins and outs of fMRI signals. *Nat. Neurosci.* 2007; 10: 1230–1232.
5. Logothetis NK. What we can do and what we cannot do with fMRI. *Nature* 2008; 453: 869–878.
6. Schulz K, Sydekum E, Krueppel R, Engelbrecht CJ, Schlegel F, Schröter A, Rudin M, Helmchen F. Simultaneous BOLD fMRI and fiber-optic calcium recording in rat neocortex. *Nat. Methods* 2012; 9: 597–602. DOI:10.1038/nmeth.2013.
7. Le Bihan D, Urayama S, Aso T, Hanakawa T, Fukuyama H. Direct and fast detection of neuronal activation in the human brain with diffusion MRI. *Proc. Natl. Acad. Sci. USA* 2006; 103: 8263–8268. DOI:10.1073/pnas.0600644103.
8. Tirosh N, Nevo U. Neuronal activity significantly reduces water displacement: DWI of a vital rat spinal cord with no hemodynamic effect. *Neuroimage* 2013; 76: 98–107. DOI:10.1016/j.neuroimage.2013.02.065.
9. Flint J, Hansen B, Vestergaard-Poulsen P, Blackband SJ. Diffusion weighted magnetic resonance imaging of neuronal activity in the hippocampal slice model. *Neuroimage* 2009; 46: 411–418. DOI:10.1016/j.neuroimage.2009.02.003.
10. Miller KL, Bulte DP, Devlin H, Robson MD, Wise RG, Woolrich MW, Jezzard P, Behrens T. Evidence for a vascular contribution to diffusion FMRI at high b value. *Proc. Natl. Acad. Sci. USA.* 2007; 104: 20967–20972. DOI:10.1073/pnas.0707257105.
11. Petridou N, Plenz D, Silva AC, Loew M, Bodurka J, Bandettini PA. Direct magnetic resonance detection of neuronal electrical activity. *Proc. Natl. Acad. Sci. USA.* 2006; 103: 16015–16020. DOI:10.1073/pnas.0603219103.
12. Bodurka J, Bandettini PA. Toward direct mapping of neuronal activity: MRI detection of ultraweak, transient magnetic field changes. *Magn. Reson. Med.* 2002; 47: 1052–1058. DOI:10.1002/mrm.10159.
13. Parkes LM, de Lange FP, Fries P, Toni I, Norris DG. Inability to directly detect magnetic field changes associated with neuronal activity. *Magn. Reson. Med.* 2007; 57: 411–416. DOI:10.1002/mrm.21129.
14. Truong T-K, Song AW. Finding neuroelectric activity under magnetic-field oscillations (NAMO) with magnetic resonance imaging in vivo. *Proc. Natl. Acad. Sci. USA.* 2006; 103: 12598–12601. DOI:10.1073/pnas.0605486103.
15. Roth BJ, Basser PJ. Mechanical model of neural tissue displacement during Lorentz effect imaging. *Magn. Reson. Med.* 2009; 61: 59–64. DOI:10.1002/mrm.21772.
16. Ng MC, Wong KK, Li G, Lai S, Yang ES, Hu Y, Luk KD. Proton-density-weighted spinal fMRI with sensorimotor stimulation at 0.2 T. *Neuroimage* 2006; 29: 995–999. DOI:10.1016/j.neuroimage.2005.08.011.
17. Jochimsen TH, Norris DG, Möller HE. Is there a change in water proton density associated with functional magnetic resonance imaging? *Magn. Reson. Med.* 2005; 53: 470–473. DOI:10.1002/mrm.20351.
18. Witzel T, Lin F-H, Rosen BR, Wald LL. Stimulus-induced Rotary Saturation (SIRS): a potential method for the detection of neuronal currents with MRI. *Neuroimage* 2008; 42: 1357–1365. DOI:10.1016/j.neuroimage.2008.05.010.
19. De Luca F. Direct fMRI by random spin-lock along the neural field. *Magn. Reson. Imaging* 2011; 29: 951–957. DOI:10.1016/j.mri.2011.04.003.
20. Li C-L, McIlwain H. Maintenance of resting membrane potentials in slices of mammalian cerebral cortex and other tissues in vitro. *J. Physiol.* 1957; 139: 178–190.
21. Yamamoto C, McIlwain H. Electrical activities in thin sections from the mammalian brain maintained in chemically-defined media in vitro. *J. Neurochem.* 1966; 13: 1333–1343.
22. Skrede KK, Westgaard RH. The transverse hippocampal slice: a well-defined cortical structure maintained in vitro. *Brain Res.* 1971; 35: 589–593. DOI:10.1016/0006-8993(71)90508-7.
23. Brooks KJ, Kauppinen RA, Williams SR, Bachelard HS, Bate TE, Gadian DG. Ammonia causes a drop in intracellular pH in metabolizing cortical brain slices. A  $[31\text{P}]$ - and  $[1\text{H}]$ nuclear magnetic resonance study. *Neuroscience* 1989; 33: 185–192. DOI:10.1016/0306-4522(89)90320-5.

24. Badar-Goffer R, Morris P, Thatcher N, Bachelard H. Excitotoxic amino acids cause appearance of magnetic resonance spectroscopy-observable zinc in supervised cortical slices. *J. Neurochem.* 2008; 62: 2488–2491. DOI:10.1046/j.1471-4159.1994.62062488.x.
25. Buckley DL, Bui JD, Phillips MI, Zelles T, Inglis BA, Plant HD, Blackband SJ. The effect of ouabain on water diffusion in the rat hippocampal slice measured by high resolution NMR imaging. *Magn. Reson. Med.* 1999; 41: 137–142. <http://www.ncbi.nlm.nih.gov/pubmed/10025621>.
26. Flint JJ, Lee CH, Hansen B, Fey M, Schmidig D, Bui JD, King MA, Vestergaard-Poulsen P, Blackband SJ. Magnetic resonance microscopy of mammalian neurons. *Neuroimage* 2009; 46: 1037–1040. DOI:10.1016/j.neuroimage.2009.03.009.
27. Shepherd TM, Blackband SJ, Wirth ED. Simultaneous diffusion MRI measurements from multiple perfused rat hippocampal slices. *Magn. Reson. Med.* 2002; 48: 565–569. DOI:10.1002/mrm.10241.
28. Shepherd TM, Scheffler B, King MA, Stanisiz GJ, Steindler DA, Blackband SJ. MR microscopy of rat hippocampal slice cultures: a novel model for studying cellular processes and chronic perturbations to tissue microstructure. *Neuroimage* 2006; 30: 780–786. DOI:10.1016/j.neuroimage.2005.10.020.
29. Cohen MM, Pettegrew JW, Kopp SJ, Minshew N, Glonek T. P-31 nuclear magnetic resonance analysis of brain: Normoxic and anoxic brain slices. *Neurochem. Res.* 1984; 9: 785–801. DOI:10.1007/BF00965666.
30. Stroman PW, Lee AS, Pitchers KK, Andrew RD. Magnetic resonance imaging of neuronal and glial swelling as an indicator of function in cerebral tissue slices. *Magn. Reson. Med.* 2008; 59: 700–706. DOI:10.1002/mrm.21534.
31. Bui JD, Buckley DL, Phillips MI, Blackband SJ. Nuclear magnetic resonance imaging measurements of water diffusion in the perfused hippocampal slice during N-methyl-D-aspartate-induced excitotoxicity. *Neuroscience* 1999; 93: 487–490. DOI:10.1016/S0306-4522(99)00191-8.
32. Shepherd TM, Thelwall PE, Blackband SJ, Pike BR, Hayes RL, Wirth ED. Diffusion magnetic resonance imaging study of a rat hippocampal slice model for acute brain injury. *J. Cereb. Blood Flow Metab.* 2003; 23: 1461–1470. DOI:10.1097/01.WCB.0000100852.67976.C2.
33. Shepherd TM, Wirth ED, Thelwall PE, Chen H-X, Roper SN, Blackband SJ. Water diffusion measurements in perfused human hippocampal slices undergoing tonic changes. *Magn. Reson. Med.* 2003; 49: 856–863. DOI:10.1002/mrm.10456.
34. Bear MF, Connors BW, Paradiso MA. *Neuroscience*. 3rd edition, Lippincott Williams & Wilkins: Baltimore, 2007.
35. Helmchen F, Konnerth A. *Imaging in Neuroscience: A Laboratory Manual*. Cold Spring Harbor Laboratory Press, New York, 2011.
36. Logothetis NK, Pauls J, Augath M, Trinath T, Oeltermann A. Neurophysiological investigation of the basis of the fMRI signal. *Nature* 2001; 412: 150–157. DOI:10.1038/35084005.
37. Kim D-S, Ronen I, Olman C, Kim S-G, Ugurbil K, Toth LJ. Spatial relationship between neuronal activity and BOLD functional MRI. *Neuroimage* 2004; 21: 876–885. DOI:10.1016/j.neuroimage.2003.10.018.
38. Wind RA, Minard KR, Holtom GR, Majors PD, Ackerman EJ, Colson SD, Cory DG, Daly DS, Ellis PD, Metting NF, Parkinson CI, Price JM, Tang XW. An integrated confocal and magnetic resonance microscope for cellular research. *J. Magn. Reson.* 2000; 147: 371–377. DOI:10.1006/jmre.2000.2212.
39. Wind RA, Majors PD, Minard KR, Ackerman EJ, Daly DS, Holtom GR, Thrall BD, Weber TJ. Combined confocal and magnetic resonance microscopy. *Appl. Magn. Reson.* 2002; 22: 145–158. DOI:10.1007/BF03166099.
40. Majors PD, Minard KR, Ackerman EJ, Holtom GR, Hopkins DF, Parkinson CI, Weber TJ, Wind RA. A combined confocal and magnetic resonance microscope for biological studies. *Rev. Sci. Instrum.* 2002; 73: 4329. DOI:10.1063/1.1517146.
41. Minard KR, Holtom GR, Kathmann LE, Majors PD, Thrall BD, Wind RA. Simultaneous 1H PFG-NMR and confocal microscopy of monolayer cell cultures: effects of apoptosis and necrosis on water diffusion and compartmentalization. *Magn. Reson. Med.* 2004; 52: 495–505. DOI:10.1002/mrm.20179.
42. Casanova F, Perlo J, Blümich B. *Single-Sided NMR*. Springer: Berlin, 2011.
43. Danieli E, Blümich B. Single-sided magnetic resonance profiling in biological and materials science. *J. Magn. Reson.* 2012; 1–13. DOI:10.1016/j.jmr.2012.11.023.
44. Rata DG, Casanova F, Perlo J, Demco DE, Blümich B. Self-diffusion measurements by a mobile single-sided NMR sensor with improved magnetic field gradient. *J. Magn. Reson.* 2006; 180: 229–235. DOI:10.1016/j.jmr.2006.02.015.
45. Haken R, Blümich B. Anisotropy in tendon investigated in vivo by a portable NMR scanner, the NMR-MOUSE. *J. Magn. Reson.* 2000; 144: 195–199. DOI:10.1006/jmre.2000.2040.
46. Rössler E, Mattea C, Mollova A, Stapf S. Low-field one-dimensional and direction-dependent relaxation imaging of bovine articular cartilage. *J. Magn. Reson.* 2011; 213: 112–118. DOI:10.1016/j.jmr.2011.09.014.
47. Bai R, Basser PJ, Briber RM, Horkay F. NMR water self-diffusion and relaxation studies on sodium polyacrylate solutions and gels in physiologic ionic solutions. *J. Appl. Polym. Sci.* 2014; 131: 1–7. DOI:10.1002/app.40001.
48. Berridge MJ, Lipp P, Bootman MD. The versatility and universality of calcium signalling. *Nat. Rev. Mol. Cell Biol.* 2000; 1: 11–21. DOI:10.1038/35036035.
49. Tsien RW, Tsien RY. Calcium channels, stores, and oscillations. *Annu. Rev. Cell Biol.* 1990; 6: 715–760. DOI:10.1146/annurev.cb.06.110190.003435.
50. Stoppini L, Buchs P-A, Muller D. A simple method for organotypic cultures of nervous tissue. *J. Neurosci. Methods* 1991; 37: 173–182. DOI:10.1016/0165-0270(91)90128-M.
51. Caeser M, Schüz A. Maturation of neurons in neocortical slice cultures: A light and electron microscopic study on in situ and in vitro material. *J. Hirnforsch.* 1992; 33: 429–443.
52. Karpiak VC, Plenz D. Preparation and maintenance of organotypic cultures for multi-electrode array recordings. *Curr. Protoc. Neurosci. Chapter* 2002; 6 Unit 6.15. DOI:10.1002/0471142301.ns0615s19.
53. Beggs JM, Plenz D. Neuronal avalanches are diverse and precise activity patterns that are stable for many hours in cortical slice cultures. *J. Neurosci.* 2004; 24: 5216–5229. DOI:10.1523/JNEUROSCI.0540-04.2004.
54. Stewart CV, Plenz D. Homeostasis of neuronal avalanches during postnatal cortex development in vitro. *J. Neurosci. Methods* 2008; 169: 405–416. DOI:10.1016/j.jneumeth.2007.10.021.
55. Daviaud N, Garbayo E, Lautram N, Franconi F, Lemaire L, Perez-Pinzon M, Montero-Menei CN. Modeling nigrostriatal degeneration in organotypic cultures, a new ex vivo model of Parkinson's disease. *Neuroscience* 2014; 256: 10–22. DOI:10.1016/j.neuroscience.2013.10.021.
56. Shriki O, Alstott J, Carver F, Holroyd T, Henson RNA, Smith ML, Coppola R, Bullmore E, Plenz D. Neuronal avalanches in the resting MEG of the human brain. *J. Neurosci.* 2013; 33: 7079–7090. DOI:10.1523/JNEUROSCI.4286-12.2013.
57. Yu S, Yang H, Nakahara H, Santos GS, Nikolić D, Plenz D. Higher-order interactions characterized in cortical activity. *J. Neurosci.* 2011; 31: 17514–17526. DOI:10.1523/JNEUROSCI.3127-11.2011.
58. Plenz D, Stewart CV, Shew W, Yang H, Klaus A, Bellay T. Multi-electrode array recordings of neuronal avalanches in organotypic cultures. *J. Vis. Exp.* 2011. DOI:10.3791/2949.
59. Song Y-Q. Categories of coherence pathways for the CPMG sequence. *J. Magn. Reson.* 2002; 157: 82–91. DOI:10.1006/jmre.2002.2577.
60. Henkelman RM, Stanisiz GJ, Kim JK, Bronskill MJ. Anisotropy of NMR properties of tissues. *Magn. Reson. Med.* 1994; 32: 592–601. <http://www.ncbi.nlm.nih.gov/pubmed/21669302>.
61. Le Bihan D. The “wet mind”: water and functional neuroimaging. *Phys. Med. Biol.* 2007; 52: 57–90. DOI:10.1088/0031-9155/52/7/R02.
62. Watzlaw J, Glöggler S, Blümich B, Mokwa W, Schnakenberg U. Stacked planar micro coils for single-sided NMR applications. *J. Magn. Reson.* 2013; 230: 176–185. DOI:10.1016/j.jmr.2013.02.013.
63. Koester HJ, Sakmann B. Calcium dynamics associated with action potentials in single nerve terminals of pyramidal cells in layer 2/3 of the young rat neocortex. *J. Physiol.* 2000; 529: 625–646. DOI:10.1111/j.1469-7793.2000.00625.x.
64. Helmchen F, Imoto K, Sakmann B. Ca<sup>2+</sup> buffering and action potential-evoked Ca<sup>2+</sup> signaling in dendrites of pyramidal neurons. *Biophys. J.* 1996; 70: 1069–1081. DOI:10.1016/S0006-3495(96)79653-4.
65. Kleinschmidt A, Obrig H, Requardt M, Merboldt KD, Dirnagl U, Villringer A, Frahm J. Simultaneous recording of cerebral blood oxygenation changes during human brain activation by magnetic resonance imaging and near-infrared spectroscopy. *J. Cereb. Blood Flow Metab.* 1996; 16: 817–826. DOI:10.1097/00004647-199609000-00006.
66. Mehagnoul-Schipper DJ, van der Kallen BFW, Colier WJNM, van der Sluijs MC, van Erning LJTO, Thijssen HOM, Oeseburg B, Hoefnagels WHL, Jansen RWMM. Simultaneous measurements of cerebral oxygenation changes during brain activation by near-

- infrared spectroscopy and functional magnetic resonance imaging in healthy young and elderly subjects. *Hum. Brain Mapp.* 2002; 16: 14–23.
67. Perlo J, Casanova F, Blumich B. 3D imaging with a single-sided sensor: an open tomograph. *J. Magn. Reson.* 2004; 166: 228–235. DOI:10.1016/j.jmr.2003.10.018.
  68. Liberman A, Bergman E, Sarda Y, Nevo U. Faster imaging with a portable unilateral NMR device. *J. Magn. Reson.* 2013; 231: 72–78. DOI:10.1016/j.jmr.2013.03.009.
  69. Bloembergen N, Purcell E, Pound R. Relaxation effects in nuclear magnetic resonance absorption. *Phys. Rev.* 1948; 73: 679–712. DOI:10.1103/PhysRev.73.679.
  70. Fischer HW, Rinck PA, van Haverbeke Y, Muller RN. Nuclear relaxation of human brain gray and white matter: Analysis of field dependence and implications for MRI. *Magn. Reson. Med.* 1990; 16: 317–334. DOI:10.1002/mrm.1910160212.
  71. Rooney WD, Johnson G, Li X, Cohen ER, Kim S-G, Ugurbil K, Springer CS. Magnetic field and tissue dependencies of human brain longitudinal  $^1\text{H}_2\text{O}$  relaxation in vivo. *Magn. Reson. Med.* 2007; 57: 308–318. DOI:10.1002/mrm.21122.
  72. Duyn JH, van Gelderen P, Li T-Q, de Zwart JA, Koretsky AP, Fukunaga M. High-field MRI of brain cortical substructure based on signal phase. *Proc. Natl. Acad. Sci. USA.* 2007; 104: 11796–11801. DOI:10.1073/pnas.0610821104.
  73. Bodurka J, Jesmanowicz A, Hyde JS, Xu H, Estkowski L, Li SJ. Current-induced magnetic resonance phase imaging. *J. Magn. Reson.* 1999; 137: 265–271. DOI:10.1006/jmre.1998.1680.
  74. Pyatigorskaya N, Le Bihan D, Reynaud O, Ciobanu L. Relationship between the diffusion time and the diffusion MRI signal observed at 17.2 tesla in the healthy rat brain cortex. *Magn. Reson. Med.* 2013; 00: 1–9. DOI:10.1002/mrm.24921.
  75. Tsurugizawa T, Ciobanu L, Le Bihan D. Water diffusion in brain cortex closely tracks underlying neuronal activity. *Proc. Natl. Acad. Sci.* 2013; 110: 11636–11641.
  76. Niendorf T, Norris DG, Leibfritz D. Detection of apparent restricted diffusion in healthy rat brain at short diffusion times. *Magn. Reson. Med.* 1994; 32: 672–677.
  77. Tasaki I. Rapid structural changes in nerve fibers and cells associated with their excitation processes. *Jpn. J. Physiol.* 1999; 49: 125–138.
  78. Fields RD, Woo DH, Basser PJ. Glial regulation of the neuronal connectome through local and long-distant communication. *Neuron* 2015; 86: 374–386. DOI:10.1016/j.neuron.2015.01.014.
  79. Hirase H, Qian L, Barthó P, Buzsáki G. Calcium dynamics of cortical astrocytic networks in vivo. *PLoS Biol.* 2004 E96; 2. DOI:10.1371/journal.pbio.0020096.
  80. Shigetomi E, Kracun S, Sofroniew MV, Khakh BS. A genetically targeted optical sensor to monitor calcium signals in astrocyte processes. *Nat. Neurosci.* 2010; 13: 759–766. DOI:10.1038/nn.2557.